Reducing Propulsion Airframe Aeroacoustic Interactions with Uniquely Tailored Chevrons: 2. Installed Nozzles

Vinod G. Mengle[*], Ronen Elkoby[†], Leon Brusniak[‡]
The Boeing Company, Seattle, WA 98124-2207

and

Russ H. Thomas[§]
NASA Langley Research Center, Hampton, VA, 23681-2199

Propulsion airframe aeroacoustic (PAA) interactions arise due to the manner in which an engine is installed on the airframe and lead to an asymmetry in the flow/acoustic environment, for example, for under-the-wing installations due to the pylon, the wing and the high-lift devices. In this work we study how we can affect these PAA interactions to reduce the overall jet-related installed noise by tailoring the chevron shapes on fan and core nozzles in a unique fashion to take advantage of this asymmetry. In part 1 of this trio of papers we introduced the concept of azimuthally varying chevrons (AVC) and showed how some types of AVCs can be more beneficial than the conventional chevrons when tested on "isolated" scaled nozzles inclusive of the pylon effect. In this paper, we continue to study the effect of installing these AVC nozzles under a typical scaled modern wing with high-lift devices placed in a free jet. The noise benefits of these installed nozzles, as well as their installation effects are systematically studied for several fan/core AVC combinations at typical take-off conditions with high bypass ratio. We show, for example, that the top-enhanced mixing T-fan AVC nozzle (with enhanced mixing near the pylon and less mixing away from it) when combined with conventional chevrons on the core nozzle is quieter than conventional chevrons on both nozzles, and hardly produces any high-frequency lift, just as in the isolated case; however, its installed nozzle benefit is less than its isolated nozzle benefit. This suppression of take-off noise benefit under installed conditions, compared to its isolated nozzle benefit, is seen for all other chevron nozzles. We show how these relative noise benefits are related to the relative installation effects of AVCs and baseline nozzles.

Nomenclature

AVC	=	azimuthally varying chevron
b	=	baseline (no chevron) round nozzle
B	=	bottom-enhanced mixing chevron nozzle
BANDN	=	$1/3^{rd}$ octave band (o.b.) number = $10*\log(1/3^{rd}$ o.b. frequency)
D	=	nozzle diameter
f	=	frequency (hz)
HFL	=	high frequency lift (increase) in sound pressure level compared to baseline nozzle
K	=	K-mixing chevron nozzle
LSAF	=	low speed aeroacoustic facility (at Boeing)
M_{wt}	=	wind-tunnel Mach number
NPR_c, NPR_f	=	nozzle pressure ratio of core (or primary) and fan (or secondary) stream, respectively
OASPL	=	overall sound pressure level (dB)
PAA	=	propulsion airframe aeroacoustics

---

[*] Engineer/Scientist, Acoustics & Fluid Mechanics Dept., P.O. Box 3707, MC: 67-ML, Sr. Member, AIAA.
[†] Engineer/Scientist, 787 Product Development Group, P.O. Box 3707, MC: OR-MM, Member, AIAA .
[‡] Engineer/Scientist, Acoustics & Fluid Mechanics Dept., P.O. Box 3707, MC: 67-ML.
[§] Senior Research Engineer, Aeroacoustics Branch, MS 166, Sr. Member, AIAA.

p_{amb}	=	ambient pressure
R	=	radial distance of polar array of microphones from the core nozzle exit center
R	=	reference state-of-the-art (azimuthally uniform) chevron nozzle
RH	=	relative humidity (%)
SPL	=	sound pressure level (dB)
T	=	ambient temperature
T	=	top-enhanced mixing chevron nozzle
TTR	=	ratio of total temperature of core to that of fan stream
V	=	variable immersion/constant chord chevron fan nozzle with K-type mixing
θ	=	microphone angle (from the inlet axis)

I.   Introduction

WHEN an engine is placed in the vicinity of an airplane the flow/acoustic interactions between them change considerably. Such interactions due to engine installation are called as Propulsion Airframe Aeroacoustic (PAA) interactions, and PAA is becoming an important and fast-growing aeroacoustics research field. The change in the flow/acoustic field can arise, for example, due to the pylon or strut used in the installation, the reflection and diffraction of engine noise by the wing and its high-lift devices, like, flaps, or the interaction of the exhaust jet and flaps which can generate new noise sources, like, jet-flap interaction noise. Our focus here is on the reduction of overall airplane noise due to the jet and its interaction with the pylon and the wings. With more and more stringent noise regulations on airplane noise at the airports, we need to seek better and better ways to reduce it, and studying different and novel ways to reduce PAA interactions directly or designing favorable PAA interactions to reduce net radiated noise can help with this noise reduction goal incrementally.

When engines are installed on an airplane, say, underneath the wing, as is typical in modern jet airplanes, there exists an inherent top-bottom asymmetry in the flow/acoustic field, for example, the pylon is only on the top side of the jet, the wing reflects engine noise from the upper side to an observer below it and the jet-flap interaction is also from one side, the top one. However, state-of-the-art chevrons used to reduce jet noise are azimuthally uniform[1, 2] and have not taken advantage of this top-bottom asymmetry to reduce jet-related noise any further. Earlier, in Part 1[3] of this study, we introduced the concept of azimuthally varying chevrons (AVC) to take advantage of this asymmetry and systematically analyzed results when such AVCs are used in "isolated" nozzles, inclusive of a pylon. This paper, which is Part 2 of this study, is a continuation of this work to examine the effects of AVCs on PAA when the nozzles are installed under the wing and compare them with the results for isolated nozzles. Part 3[4] focuses on jet-flap interaction noise for AVC nozzles under installed conditions and is complementary to this paper. (The other two parts of this series, henceforth will be simply referred to as Part 1 and Part 3).

This work is part of a bigger PAA-related NASA and Boeing partnership under the Quiet Technology Demonstrator 2 program. An overview of QTD2 project is given in Herkes et al[5]. Most of the relevant references on PAA work with and without chevrons, and the AVC concept can be found in Part 1 and will not be repeated here; the reader is urged to read this paper in conjunction with Part 1 for a more complete understanding. Briefly, in Part 1, we introduced, designed and tested scale models of different azimuthally varying chevrons, like, the top- or the bottom-enhanced mixing chevrons which, as the names imply, are supposed to enhance the mixing between the two streams around the chevrons at the top near the pylon or away from it. Conventional chevrons, it may be recalled, are azimuthally uniform, that is, do not vary in shape or size from chevron to chevron. These tests were conducted in Boeing's low speed aeroacoustics facility (LSAF) with a free jet. We discovered in Part 1 that certain types of AVCs, like the top-enhanced mixing T-fan chevrons, are quieter than the conventional state-of-the-art chevrons when tested as isolated nozzles with a pylon. Importantly, this occurred without any appreciable high-frequency lift (HFL), which is otherwise endemic to the conventional chevrons and reduce their noise benefits due to larger noy penalty at higher frequencies. Hence, it is important to study these AVCs under installed nozzle conditions and compare their relative advantages, if any, and how they change due to installation.

In the next few sections, we briefly explain the additional types of AVC nozzles that were tested under installed conditions and the installed experimental setup in LSAF. Next we present and discuss the experimental results to study the effects of fan AVCs and core AVCs on installed noise benefits, as well as on the installation effects.

American Institute of Aeronautics and Astronautics

II.   Nozzle Models and Experimental Setup

A. Nozzle Models

In addition to the AVC nozzles used in the companion isolated test of Part 1, we designed and built a couple more AVCs which were tested under installed conditions. In the isolated test we used the T- and the B-chevrons which had enhanced mixing, respectively, on the top-side (near the pylon) and the bottom-side (away from the pylon). Each of these AVC nozzles also had less mixing on their other diametrically opposite side to reduce the high frequency increase, and loss of thrust and discharge coefficients which can arise due to higher axial vorticity generated by larger chevron immersions or lengths. This azimuthally varying mixing was implemented, as explained in Part 1, by using linearly varying chevron lengths and immersions from top to bottom. In addition, for comparison we also had the reference state-of-the-art azimuthally uniform chevrons, R, and the baseline simple splitter nozzle, b.

Another possibility we wanted to explore in this installed test was with enhanced mixing on both top and bottom sides but less mixing in the middle – giving a sort of K-shaped mixing when viewed from the side. We built two types of AVCs to implement this idea: one with "K-shaped" chevron lengths, as well as K-shaped immersions, that is, chevrons with higher chord lengths and immersions at top and bottom but less in the middle; the second type was with constant chevron chord lengths but variable "K-shaped" immersions. In both cases, the chevron lengths and immersions were linearly distributed from middle to top or middle to bottom. However, note that the distribution of chevrons in these scaled nozzles is not symmetric about the horizontal axis because of unequal non-usable azimuthal regions (stay-out zones) at the top and bottom due to the pylon and also the thrust reverser sleeves which are used in practical applications. We will call these respectively, K-chevrons and V-chevrons. For the sake of comparison with the previous R- and T-chevron nozzles, the number of chevrons in K and V nozzles was kept the same - 16 chevrons for the fan nozzle and 8 chevrons for the core nozzle. These are one-point designs and, due to lack of time, were designed with only rudimentary one-dimensional analysis to approximately match the mass-flow rates at cruise conditions. No optimization was done as we were simply trying to study if this type of azimuthal variation in mixing makes any reduction in total noise and PAA interaction effects.

Thus, in total, we had the baseline simple splitter nozzle, b, the conventional R-chevrons, and the azimuthally varying T-, B-, and K- chevrons for both the fan and the core nozzles, and the V-chevrons for only the fan nozzle. These were built as chevron nozzle rings so that interchanging them during the test was convenient. A schematic of a few possible combinations of these nozzles is shown in Fig. 1 and a group photo can be found in Part 3 (Fig. 2).
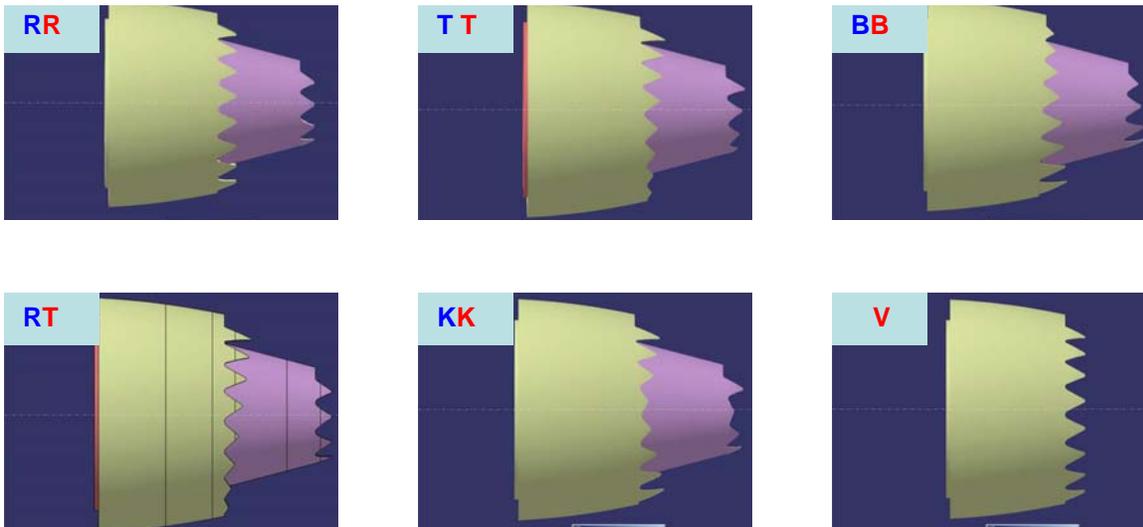
Figure 1.   Examples of combinations of the AVCs for both fan and core nozzles (the first symbol in blue is for the core nozzle and the second in red is for the fan nozzle). The fan/core AVC nozzle combinations which were actually tested in installed configuration are given in Table 1.

B. Experimental Setup

All these nozzle combinations were tested in the NTL3800 jet noise simulator in Boeing's Low Speed Aeroacoustic Facility (LSAF). A brief description of LSAF, the jet rig, the microphone arrays and acoustic data processing can be found in Part 1. Although the phased microphone array was used during the installed nozzle test for source diagnostics those results are not discussed here but are postponed to Part 3 and should be viewed as complementary to the results given in this paper.

For the installed test, we decided to use, for several logistic reasons, an existing scale model of a typical modern large twin-engined airplane with under-the-wing nozzle arrangement: it had a fuselage and a wing with all the high-lift devices, namely, inboard and outboard flaps, flaperon which was right behind the nozzle centered on the nozzle axis, and the leading edge slats. These high lift-devices also came in several different sets, each for a different flap detent angle to be used in approach, take-off or cruise conditions. The results for a take-off flap detent angle of only 5º are analyzed in this paper.
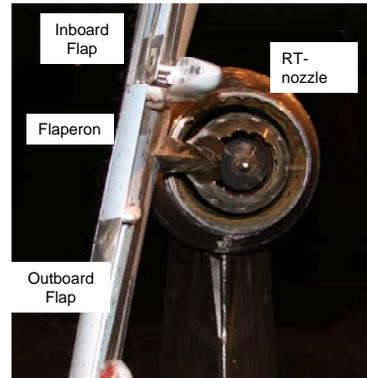

(a) View from the west side

(b) View from the east side

(c) View from inside the wind-tunnel

(d) Aft view looking towards the wind-tunnel

Figure 2. Several different views of the installed nozzle set-up showing the fuselage and the left wing with high-lift devices (inboard/outboard flaps, flaperon and leading-edge slats) at take-off flap detent of 5º. (Only the basic straight-edged flaperon shown in (d) was used for this paper.)

One issue that needed resolution at the start of the test was the orientation of the wing – whether it should be vertical or horizontal, since the wind-tunnel in which the nozzle jet rig was mounted was large enough (10 ft width by 7 ft height) to accommodate it either way. Considering that we wanted to have the far field microphones at the largest possible distance away from the installed nozzle to achieve some semblance of "far field", we decided to keep the left wing in nominally a vertical orientation so that the horizontal microphone array could be placed horizontally as far away from the nozzle as possible in the LSAF. The polar array of microphones was on a circular arc of 25 ft radius centered on the core nozzle exit plane center giving $R/D_{fan} = 32.1$ and $R/D_{core} = 68.7$. The ratio of wing chord (at nozzle axis span station) to fan diameter is 2.35 approximately. The wing also has a small dihedral angle of 6º so that is at 6º to the vertical plane. This arrangement also turned out to be conducive to arranging a right-angled support strut from the fuselage at the top with minimal torque load. The airframe support strut was

partially in the wind-tunnel flow but was streamlined and relatively thick so as not to interfere with the installed noise spectrum of interest and was on the side opposite to that of the far field microphone array.

Finally, this whole arrangement with the wing attached to the nozzle on the jet rig and the fuselage was kept at zero angle of attack to the wind-tunnel flow because creating a positive angle of attack, which is actually the case during take-off conditions to be simulated here, would have led to serious other structural, extraneous noise and jet-rig support-strut wake problems. Figures 2(a-c) show several views (photos) of this final installation from the two sides (west and east) and from inside the wind-tunnel. Figure 2(d) also shows a close-up aft view of the flaperon and flaps downstream of the installed nozzle. Note that the leading-edge slats were not deployed at take-off detent but were rather kept in "closed" cruise detent positions. Although, we also have a thrust measurement stand for measuring the forces and moments on the nozzle, it was disconnected during this installed test due to the extraneous loads from the attachment of the wing to the nozzle, in spite of this attachment of the wing to the pylon having a sliding feature.

III. Experimental Results and Discussion

Table 1 shows the various chevron and baseline nozzle combinations that were tested in the installed nozzle configuration. It should be noted that the installed test repo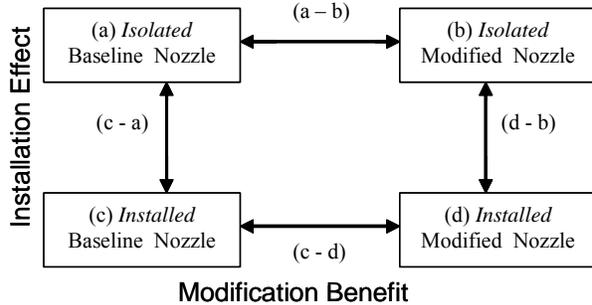rted here was chronologically done *before* the isolated test of Part 1 for certain logistic reasons, like availability of the installed nozzle setup at the beginning of the LSAF test program, etc. It is possible to extract the acoustic effect of, say, the fan AVC nozzles by keeping the core nozzle the same, such as, R or T; or, to study the effect of the core AVC nozzles by keeping the fan nozzle the same, such as, b, R , T or K. Some of these effects are analyzed here. Also note from Table 1 that some of the nozzle combinations were done both in the installed configuration as well as the isolated configuration, such as, bb, RR, RT, TT and BR, so that the differences due to installation (installation effect = SPL(installed) – SPL(isolated)) can be examined for them.

Table 1. Installed nozzle test matrix of combinations of core and fan chevron nozzles (nozzles in "bold" letters were also tested as isolated nozzles)

FAN CORE	b	R	T	B	K	V
b	bb					
R	Rb	**RR**	**RT**	RB	RK	RV
T		TR	**TT**		TK	
B		**BR**				
K		KR				

Most of these nozzles were tested for six engine cycle conditions typical of modern high bypass turbofan engines covering mainly high and low-power take-off conditions at wind-tunnel Mach numbers of M_{wt} = 0.0 and 0.30, and also three low-power approach conditions at M_{wt} = 0.0 and 0.24 for studying the effect on community noise. However, in this paper results for only one take-off power condition, which is the same as that in Part 1, are analyzed here, namely, NPR_f = 1.735, NPR_c = 1.622 and TTR = 2.513 at M_{wt} = 0.30. The nominal values of relevant non-dimensional ratios, like, velocity ratios, bypass ratio, etc. are given in Part 1.

Before we present the installed nozzle results, it is better to summarize the relation between the various isolated and installed SPL differences. For this, we introduce the four-square difference chart as shown in Fig. 3. All the fo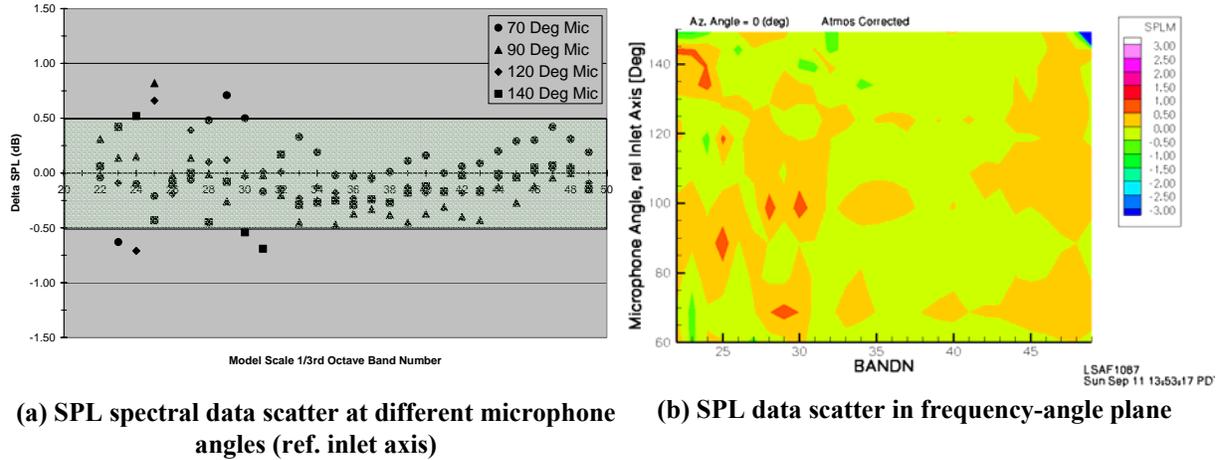ur principal configurations form the corners of this chart, namely, *isolated* baseline or modified nozzle, and *installed* baseline or modified nozzle. The modification benefit is the SPL difference in a given row, (baseline - modified), and the installation effect is the differences in a given column, (installed – isolated), as shown. In this section, we will basically study the installed noise benefits (c-d), and the installation effects (d-b). Part 1 previously dealt with the isolated noise benefits of AVCs given by (a-b) in this 4-square chart.

Figure 3. The four-square noise difference chart for installation effects: (c-a) or (d-b), and modified nozzle benefits: (a-b) or (c-d).

A. Data Repeatability and Wind-Tunnel Noise

Before we present the actual results for the installed noise benefit etc. we will consider here the repeatability of data with the wind-tunnel flow on, and the wind-tunnel noise itself. Test conditions for the baseline (bb) configuration and some AVC nozzles were repeated throughout the test period to find the limit on data scatter at different frequencies and angles. All the far field test data was normalized to the standard acoustic day conditions (T = 77º F, RH = 70%, p_{amb} = 14.7 psi) using the well-known Bass-Shield atmospheric corrections (see comments on this in Part 1) so that comparisons could be made between any two configurations.

(a) SPL spectral data scatter at different microphone angles (ref. inlet axis)

(b) SPL data scatter in frequency-angle plane

Figure 4. Data repeatability between two runs (191 and 199) for the installed baseline configuration at take-off sideline power conditions (216) with the wind-tunnel at M_{wt} = 0.30.

Figure 4 shows an example of such SPL data scatter for the installed baseline nozzle, bb, with free jet Mach Number, M_{wt} = 0.30, for two repeat tests a day apart: it shows that, except for a few outliers, the SPL scatter for bands beyond 27 is within ±0.5 dB for all microphone angles shown. The data for bands beyond 47 showed more scatter in some data due to sensitivity to atmospheric corrections. This was seen in all the repeat tests with other configurations. So we consider ±0.5 dB as the error band for SPL data within 1/3rd octave-band numbers 27 and 47 for all angles for this test, as in the isolated nozzle test of Part 1

Figure 5(a) shows SPL comparison of the wind-tunnel noise floors for the installed baseline case and the isolated baseline case with M_{wt} = 0.30. The tunnel noise floor for the isolated nozzle also includes the noise from the strut that supports the jet rig (see Fig. 2(c)). Similarly, note that the second case of installed nozzle in the wind-tunnel (without the model jet being on) is not just wind-tunnel noise floor but actually represents the change due to the presence of the wing with the high-lift devices, the fuselage and also the airframe support strut (see Figs. 2(a) and 2(c)), and, hence, represents airframe noise including airframe support strut noise. The difference between the installed and the isolated "noise floors," plotted in Fig. 5(b), shows where this "airframe + strut" noise is above the tunnel noise floor – the larger difference, like 5 dB and above, is seen to be in the low frequencies (band 25 to 30) across a wide range of front and aft angles. In other spectral-directivity regions the tunnel noise contaminates this (airframe + strut) noise, as also seen from Fig. 5(a).

More pertinent to this paper, however, is the SPL difference between the installed nozzle noise (the acoustic signal of interest) and the tunnel noise floor as shown in Fig. 5(c). If we assume that it is acceptable to have the installed noise, say, 6 dB above the tunnel noise floor then this plot immediately tells us the non-acceptable region in the spectral-directivity plane – that is seen to be at low frequencies below band 25. If we were to impose a stricter 8 dB difference, instead of 6 dB, then we see that in addition to increasing the non-acceptable lower band number limit there are also "bottle-necks" appearing in the high frequency range near band 43 for both the far upstream angles and the very shallow angles (light blue) – these "bottle-necks" are also clearly captured in the line plots of Fig. 5(a). Note, however, that the spectral-directivity region where the jet noise dominates – aft quadrant, low frequency around band 30 - the installed noise is far above the tunnel noise floor, so that changes in jet noise due to say, chevrons should be well captured.
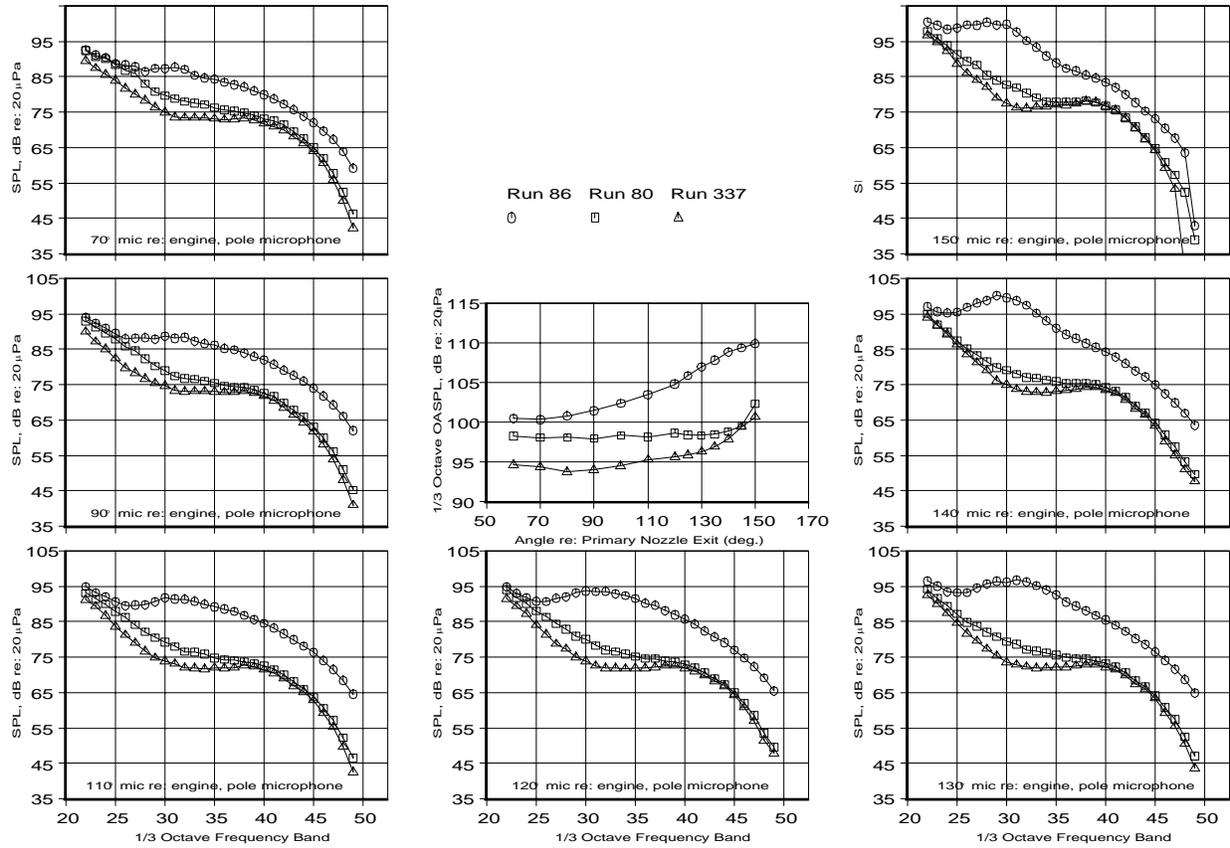
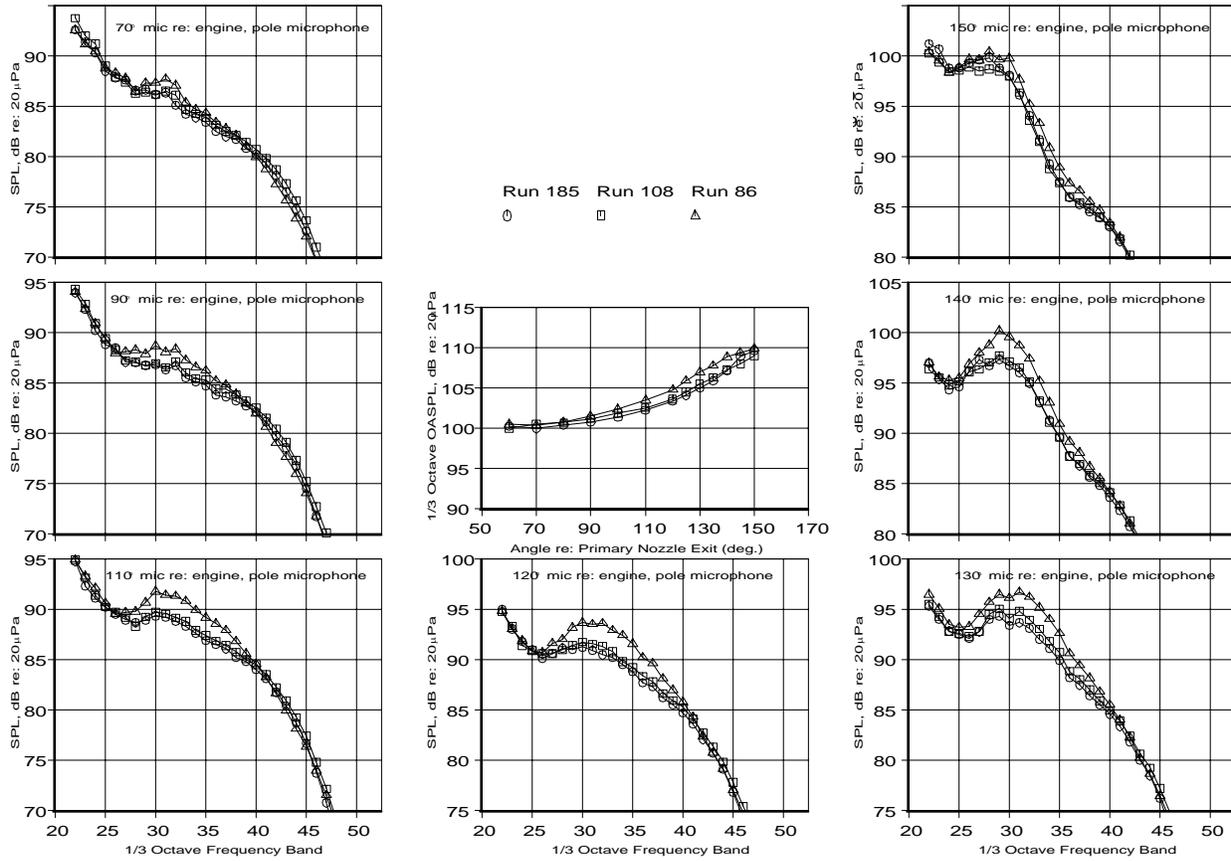**(a) Spectral comparison at different angles**
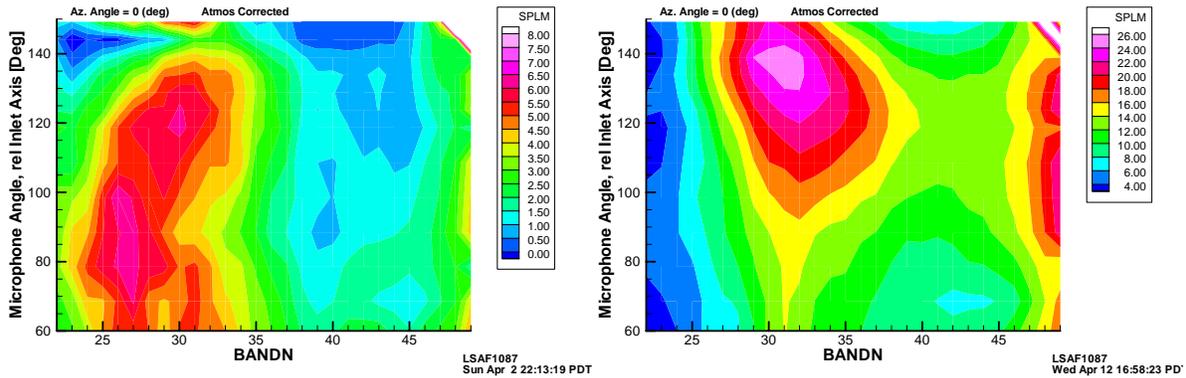
(b) SPL difference between installed and isolated wind-tunnel noise floors at $M_{wt} = 0.30$ (run 80 – run 337)

**(c) SPL difference installed noise and isolated wind-tunnel noise floor (run 86 – run 337)**

Figure 5. Comparison of wind-tunnel noise floor with isolated baseline (bb) nozzle (run 337), wind-tunnel noise floor with installed baseline nozzle (run 80), and total installed noise with baseline nozzle (run 86) at take-off sideline power conditions and wind-tunnel Mach number, $M_{wt} = 0.30$.

In general, for this high power take-off condition and the previous data repeatability criterion, restricting us to a band range between 27 and 47, the installed noise is well above the tunnel noise for all angles and is of an acceptable quality.

C. Installed Fan AVC Effect

**(a) SPL spectral comparison at various directivity angles and OASPL directivity**
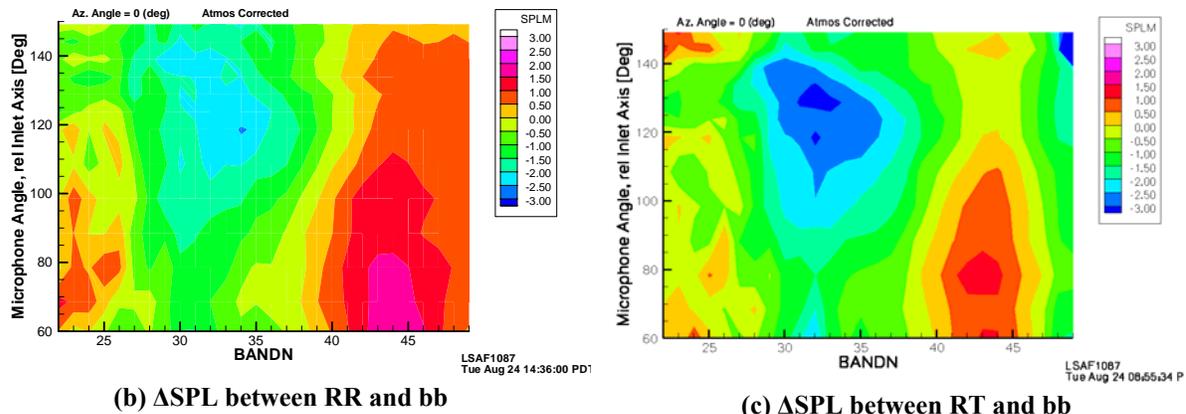
(b) ΔSPL between RR and bb

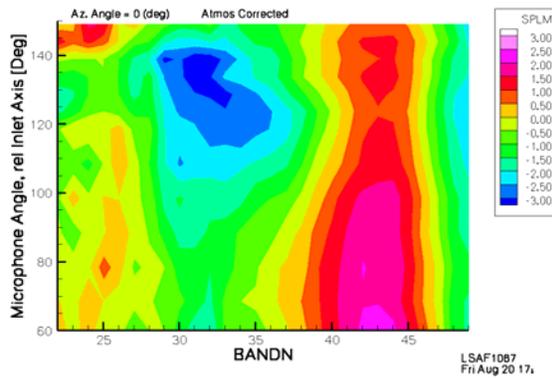**(c) ΔSPL between RT and bb**

Figure 6. Installed nozzle SPL comparison between RT (run 185), RR (run 108) and baseline, bb (run 86) nozzles at take-off sideline power conditions with $M_{wt} = 0.3$.
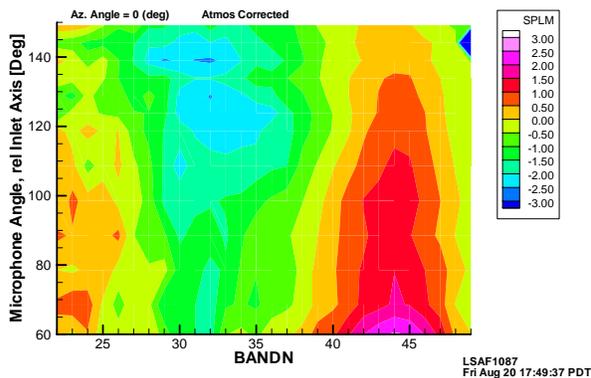
Since the isolated nozzle test in Part 1 showed that the RT-nozzle was the quietest amongst the AVC combinations tested let us first study the installed RT-nozzle. We will compare the installed RT-nozzle with the conventional chevron RR-nozzle and the baseline bb-nozzle. From Fig. 6 we note that:
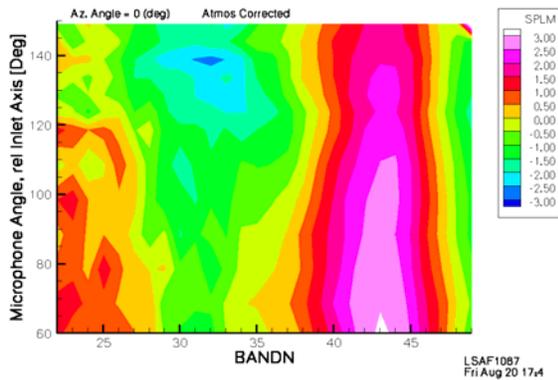
(a) ΔSPL between RB and bb

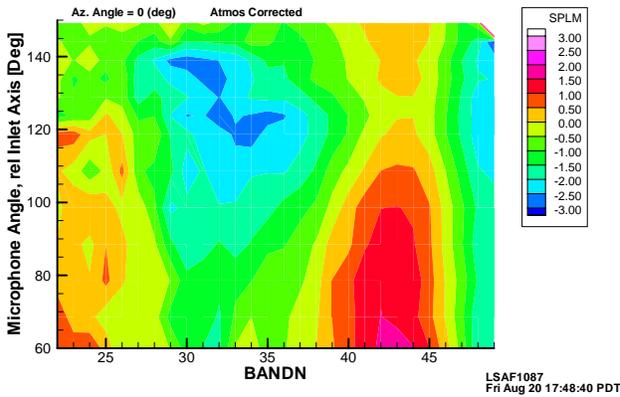

(b) ΔSPL between RK and bb

(c) ΔSPL between RV and bb

Figure 7. Installed fan AVC effect (B vs. K vs. V) with R-core chevrons held constant at take-off sideline power conditions with $M_{wt} = 0.30$.

a) From Figs. 6(a) and 6(b), the installed RR-nozzle reduces the noise compared to the baseline nozzle, bb, for frequencies below band 40 up to a maximum of 2 to 2.5 dB in the aft quadrant; but there is a high frequency lift (HFL) in SPL beyond band 40 and particularly so in the front quadrant. This is typically the case for conventional chevrons.

b) Comparison of the installed RR-case with its isolated counterpart in Fig. 8(b) of Part 1 shows that the maximum low-frequency noise benefit has decreased for the installed case by about 0.5 dB and the angle where this maximum reduction takes place has moved slightly upstream; on the contrary, the HFL for the installed case has decreased in its peak amplitude in the front quadrant and the frequency where the maximum HFL occurs has lowered in value.

c) Turning our attention now to the installed RT-nozzle, we find from Figs. 6(a) and 6(c) that, in general, it is quieter than the installed conventional RR-nozzle both in terms of low frequency reduction and reduction in HFL. This is consistent with what was observed in the isolated RT-case (compare with Fig. 8(a) and 8(c) in Ref. 3).

d) Compared to the baseline nozzle, Fig. 6(c) shows that installed RT-nozzle decreases noise by up to 3 dB near 130°, an area usually dominated by jet noise; the installed HFL is almost non-existent at the shallow angles, and reaches a maximum value of only 1 dB or so in the front quadrant; recall that the front quadrant, for turbofan engines, is usually dominated by non-jet noise sources, such as, fan noise at high frequencies and such a small increase may be immaterial; in any case, note from Fig. 6(a) that the SPL at high frequencies is far below the peak SPL at any given angle.

e) Finally, when we compare the installed RT-nozzle with its isolated counterpart (compare Fig. 6(c) here to Fig. 8(c) of Part 1), we see that the installed noise benefit of RT-nozzle over the baseline nozzle is decreased – from a maximum of about 3.8 dB to 3+ dB; there is also a decrease in the noise benefit footprint area in the spectral-directivity plane. Same is true of the conventional RR-nozzle.

f) Thus, installing the nozzle underneath the wing appears to reduce the noise benefit of both types of chevrons, regular RR- and RT-fan chevrons, at least, at take-off conditions.

Now let us study the effect of replacing the T-fan nozzle by the B-, K- and V-chevron fan nozzles but keep the core chevron nozzle the same, namely, the conventional R-core chevrons. This leads us to a comparison of RB, RK and RV nozzles. Figure 7 shows the SPL differences of these AVC nozzle combinations with the baseline nozzle at the same take-off power

9
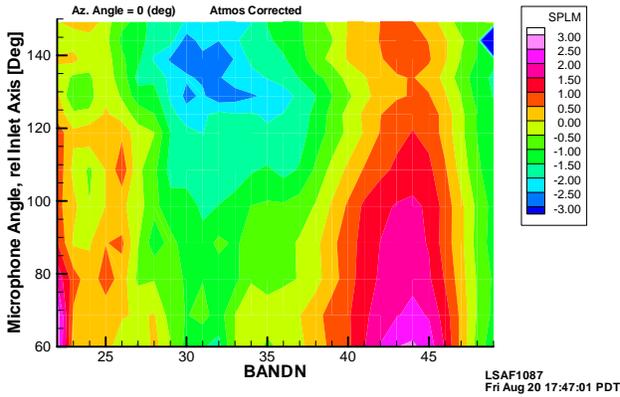
(a) ΔSPL between TR and bb

(b) ΔSPL between TT and bb
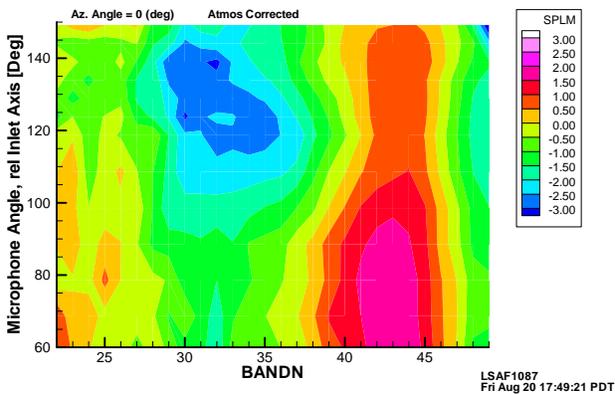
(c) ΔSPL between TK and bb

Figure 8. Installed fan AVC effect (R vs. T vs. K) with T-core chevrons held constant at take-off sideline power conditions with M_{wt} = 0.30.

condition as before and at M_{wt} = 0.30. From Fig. 7 we note that:

a) RB and RV show noise reduction of maximum 2 to 2.5 dB in the low frequencies, similar to the conventional RR-nozzle (see Fig. 6(b)), but RB has higher HFL and RV has lower HFL than RR. Thus, RB-nozzle with a B-fan nozzle (bottom-enhanced mixing) does not appear preferable; but RV nozzle, with a variable immersion fan nozzle which is designed to give K-type mixing (that is, both top and bottom enhanced mixing but less in the middle) appears to be slightly more beneficial over the conventional RR-nozzle due to its lower HFL.

b) RK-nozzle (Fig. 7(b)), on the other hand, shows more noise reduction in the low frequencies than RR-nozzle and is similar to RT-nozzle in that respect; however, it has a much higher HFL than RT-nozzle. Note that the K-mixing in the K-fan nozzle was achieved by changing both the chevron lengths and immersions, as opposed to the K-mixing in V-fan chevrons, which was achieved with only variable immersions but same chevron lengths. But note that the K-mixing achieved downstream by both of them (K- and V-nozzles) may not be the same as the equivalence between chevron lengths and chevron immersions is not known and was not calculated. It is possible that some more immersion of the V-fan chevrons could have lowered the low frequency further and increased the higher frequency further, making it comparable to the RK-noise signature (compare Figs. 7(b) and 7(c)).

Finally, let us compare the effect of fan AVCs by keeping the T-core chevrons the same (see the third row in Table 1): TR, TT and TK nozzle combinations. Figure 8 shows the SPL difference for these nozzles compared to the baseline nozzle, bb, at the same take-off conditions and M_{wt} = 0.30. We note that:

a) All of these installed nozzles give a reasonable low frequency noise reduction of up to 3 dB in the spectral-directivity region, with the TK-nozzle giving a little bit better noise reduction, comparable to RK (Fig. 7(b)).

b) However, all of them give HFL and more so in the aft quadrant, with TT-nozzle (which has the T-fan chevrons) giving the least amount of HFL

c) Comparing them to the conventional RR-nozzle (see Fig. 6(c)) it appears that all of them may be slightly better than RR in terms of both low frequency reduction and lower HFL; also, the HFL centroid for these nozzles appears to have shifted to lower frequencies compared to RR's; these generic observations may have more to do with the T-core chevron commonality than the variability due to the fan chevrons.

It would be nice to see if the installed effects of fan AVC are similar to their effects when used in isolated nozzles; but comparing the two test matrices in the two tests (compare Table 1 here with Table 1 in Part 1) shows that, unfortunately, there is no overlap to study this effect, other than the RR- and RT-nozzles which have already been studied and found to have a similar effect.

C. Installed Core AVC Effect

From Table 1, we see that we can study this effect, keeping fan nozzle the same, from nozzle combinations in three columns, namely, (i) RR vs. TR vs. BR vs. KR, and (ii) RT vs. TT, and (iii) RK vs. TK. Most of the SPL difference results in comparison to the baseline nozzle have already been shown earlier for these nozzle combinations, except for BR and KR-nozzles which are shown in Fig. 9.

(a) ΔSPL between BR and bb   (b) ΔSPL between KR and bb
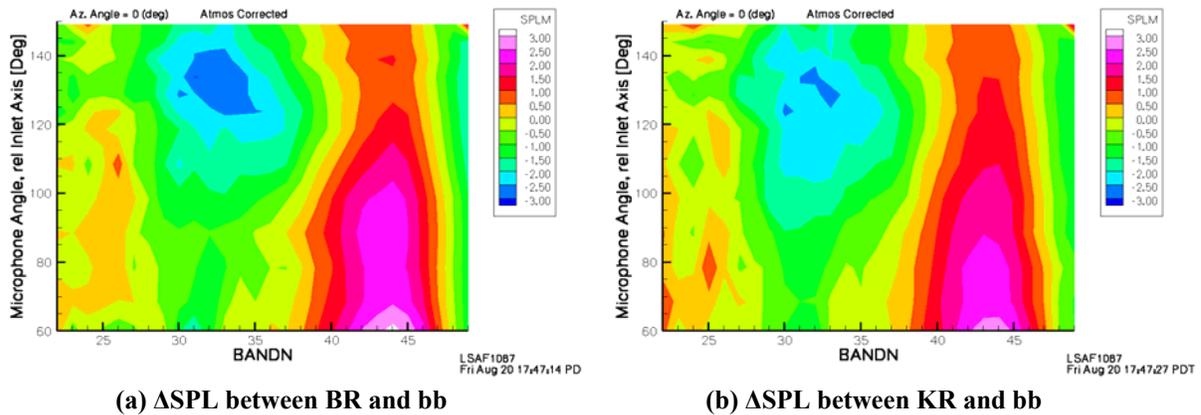
Figure 9. Installed core AVC effect (B vs. K) with R-core chevrons held constant at take-off sideline power conditions with M$_{wt}$ = 0.30.

The effect of holding fan chevrons constant as the conventional R, but changing the core chevrons can be found by comparing RR, TR, BR and KR from Figs. 6(b), 8(a), 9(a) and 9(b), respectively. We note the following:
a) T- and B-core chevrons slightly improve the low frequency noise reduction compared to the conventional R-core chevrons (by about 0.5 dB), but K-core chevrons are very similar to R-core chevrons
b) HFL for T-, B- and K-core chevrons is quite similar and only somewhat worse than the conventional R-core chevrons; since the common element in all these nozzles is the R-fan chevrons, it is most likely the case that the HFL is being caused by the R-fan chevrons and governed only to a smaller extent by the core chevrons in these cases. Recall, that when the fan chevrons were changed earlier from R to T (comparing RR to RT) the HFL reduced considerably. This makes it more likely for the HFL to be associated with the R-fan chevrons here.

Next consider the effect of holding the fan nozzle constant as T-fan chevrons and changing the core chevrons from R to T, that is, compare RT vs. TT. From Figs. 6(c) and 8(b) we see that replacing the conventional R-core with T-core chevrons reduces the low frequency benefit a little bit and increases HFL slightly; hence, these T-core chevrons are not to be preferred in this combination.

D. Installation Effect at Take-Off

Now we will study the far field SPL difference between the installed nozzle and the isolated nozzle (reported in Part 1) for a given configuration at this take-off condition with flap detent of 5º and tunnel Mach number of 0.30. This difference is usually called as the "installation effect," however, note that our isolated nozzle already includes the effect of the pylon too. The installation effect is known[6] to be large at approach conditions where the flap angles are much larger and the jet-flap interaction is higher. From Table 1 we see that only few nozzle combinations were tested in both installed and isolated configurations, so that we can study the installation effect only for those combinations, namely, bb, RR, RT, TT and BR.

Figure 10 shows this installation effect for the first four nozzle combinations as SPL-difference contour plots over the whole spectral-directivity plane using the same color scale for convenience. The common feature for all these nozzles is the dominance of the installation effect (say, above 3 dB difference) in the front quadrant for lower frequencies (up to band 32 or so). Note that the magnitude of this SPL difference is far above any repeatability

errors for lower frequencies (below band 27) but wind-tunnel noise also starts contaminating it at the very low frequencies, as seen from Fig. 5(a). The very low frequency noise cannot be attributed to the airplane-supporting strut noise because it changes with the nozzle combination and the nozzles cannot affect the strut noise because the strut is not in the downstream wake of the model jet plume and both are quite far apart (see Fig. 2).

(a) bb

(b) RR

(c) RT

(d) TT
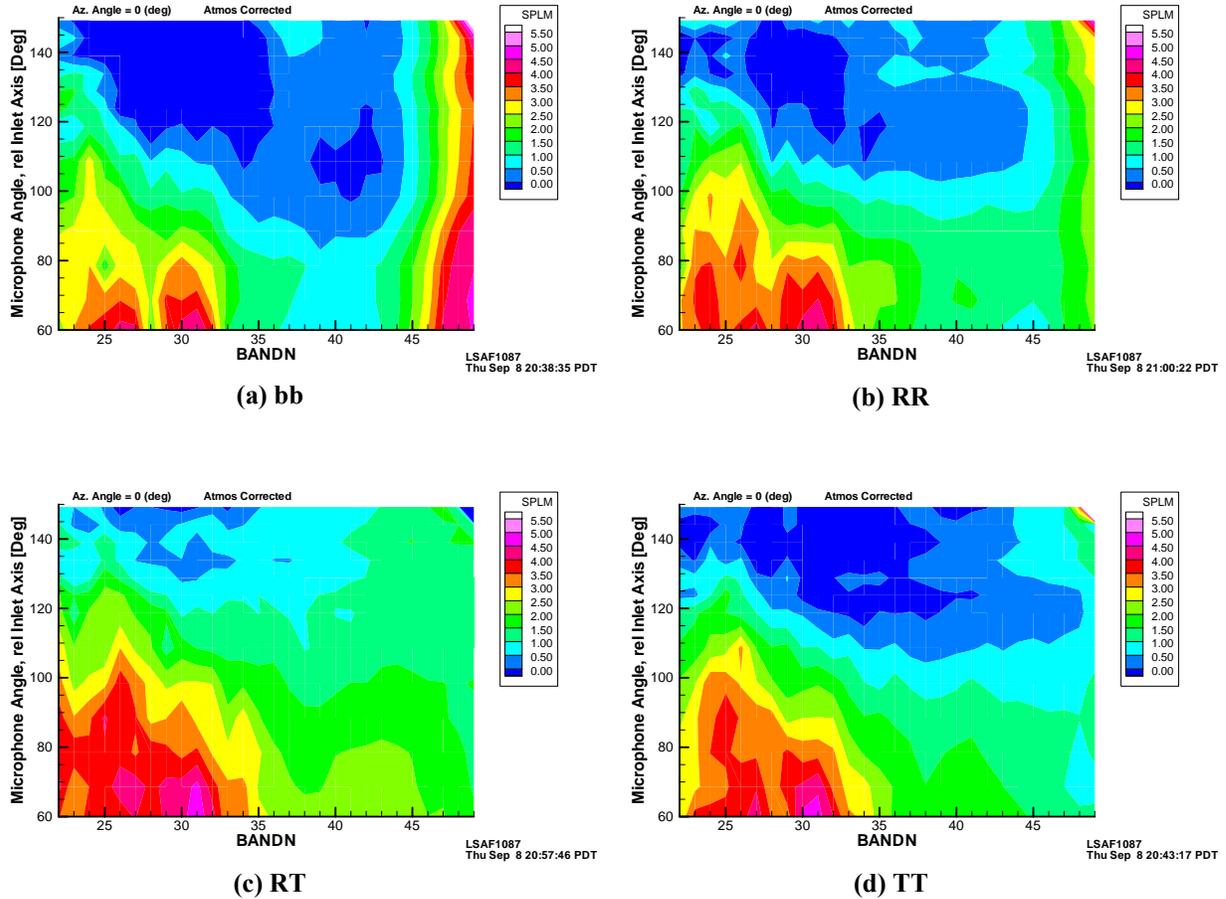
Figure 10. Installation effect, [SPL(installed) – SPL(isolated)], for four nozzle combinations at take-off sideline power conditions with $M_{wt} = 0.30$.

The installation effect in this spectral-directivity region has been attributed earlier[6,7] to the reflection and diffraction of jet noise from the wing and the high-lift devices, and the additional generation of noise due to turbulent eddies passing near the flap/flaperon side-edges and trailing edges (which can radiate noise predominantly in the front arc). However, note that the flap/flaperon deflection at take-off is small (only 5º or so), hence, this effect cannot be as large as in approach conditions where the flap deflections are much higher (30º or so). For observers below the wing, the wing itself acts like a reflector for any noise sources underneath it, especially, when their wavelength is much shorter than the wing's chord length. Jet noise sources directly underneath the wing and axially close to its mid-chord location will be reflected to both front and rear arcs in a similar fashion (even after accounting for convection due to the tunnel flow), but those near or downstream of its trailing edge will be reflected more to the front arc than the rear. Hence, the implication of the 5 dB or so installation effect in the front arc and less in the rear arc, shown in Fig. 10, is that the dominant sources must be closer to the trailing edge of the wing and can be generated at either the flap/flaperon edge itself or reflection of jet noise sources in that region. Since for band 30 (1000 hz), the wavelength to chord ratio is approximately only 0.6, but is higher than 1 for the lower bands where this effect is quite dominant, it must be more of the jet-flap interaction noise than the reflection due to the wing that must be the cause of this installation effect at take-off power. A source diagnostics study of these installation effects is beyond the scope of this paper, due to space limitations, but is presented in Part 3 where the installation effects at approach condition are also studied.

Secondly, from Figure 10, the "footprint" of this installation effect in the spectral-directivity plane (that is, the size or area of the region of the ΔSPL-contour of a certain value, say, 3 dB) appears highest for the RT-nozzle and least for the baseline nozzle, with the other two configurations, RR and TT, having an intermediate level. This seems exactly in the reverse order of their installed noise benefits. This may appear to contradict with the previous result that the total installed noise reduction for RT-nozzle, compared to the baseline nozzle, is the highest (3+ dB) at low frequencies (see Fig. 6(c)) and somewhat lower (2 to 2.5 dB) for RR and TT (see Figs. 6(b) and 8(b)). These low frequency reductions, however, are all in the aft arc, whereas, this installation effect is prominent in the front arc where these chevron nozzles have only a smaller installed benefit of about 1 to 1.5 dB.

This enlarged footprint for the installation effect of chevron nozzles at take-off actually goes hand in hand with their relative installed and isolated noise benefits compared to the baseline nozzle, and can be easily explained using the four-square difference chart introduced earlier (see Fig. 3):

a) For any frequency (f) and angle (θ) we have the isolated and installed noise benefits for the modified nozzle with respect to the baseline nozzle defined as (a-b) and (c-d), respectively.

b) Now if the isolated nozzle benefit is higher than the installed nozzle benefit at that f and θ, that is, $(a-b) > (c-d)$ then it implies that $(d-b) > (c-a)$. From Fig. 3, we see that both the sides in this latter inequality are simply the installation effects for, respectively, the modified nozzle and the baseline nozzle. Hence, this result implies that <u>if the isolated nozzle benefit is higher than the installed nozzle benefit for a modified nozzle at a given (f, θ) then its installation effect must be higher than that for the baseline nozzle at that (f, θ)</u>.

c) Conversely, if the installed benefit is higher than the isolated benefit, then the installation effect for the modified nozzle should be less than that for the baseline nozzle; in addition, of course, when the isolated benefit is equal to the installed benefit then the installation effects for the modified and the baseline nozzle should be the same.

d) These results can obviously applied in reverse order, that is, if the installation effect for the modified nozzle is higher than that for the baseline nozzle, then the isolated benefit of the modified nozzle must be higher than its installed benefit, and so on.

e) This argument can be applied at different (f, θ) points covering any region in the f-θ plane to get a comparative value for the size of the footprint for the modified nozzle and the baseline nozzle.

As an example, let us apply this argument to the case of RT-nozzle. For, say, 110º at band 30, comparison of the line plots in Fig. 6(a) here and Fig. 8(a) of Part 1 shows that the isolated benefit for RT is more than its installed benefit at least by about 1 dB (which is above the data scatter band of 0.5 dB). From the above argument this would imply that the installation effect of RT should be higher than that of the baseline at 110º and band 30: comparisons of Figs. 10(c) and 10(a) indeed proves that to be the case. Again, we can verify the same conclusion at 70º and band 30, for example, and so on. The same is found to hold good also for all other configurations.

The above argument using the four-square difference chart of Fig. 3 only gives an equivalence of relative noise benefits and relative installation effects for the modified nozzles and the baseline nozzle, but does not tell us the reason why, for example, the installed noise benefit for a modified nozzle is less (or more) than the isolated noise benefit. For that we need to get back to the flow-physics of the problem and check whether the noise benefit is more due to the reduction in jet noise source in the exhaust plume or the jet-flap interaction. These source diagnostics issues are dealt with in Part 3 for take-off as well as approach conditions using phased microphone arrays.

IV.   Conclusion

In this paper, we analyzed the far field acoustic effect of azimuthally varying chevrons, both on the fan nozzles and/or the core nozzles, under installed conditions with high-lift devices on the wing at take-off power in a free jet. As found in Part 1 for isolated nozzles, there are several fan/core AVC combinations that were found to give better low frequency noise reduction than the conventional state-of-the-art chevron nozzle with slight variations in high frequency lift (HFL). One particular fan AVC nozzle, the T-fan chevrons, in combination with the conventional R-core chevrons, again stands apart from all other nozzles, including the conventional chevrons, in terms of highest low frequency noise reduction in the aft arc and very little HFL in the front arc. However, its noise benefit under installed conditions is less than that in the isolated conditions. Installation of the nozzle under the wing appears to reduce the noise benefit, in general, for all chevron nozzles studied compared to their isolated nozzle benefit at take-off conditions.

The installation effect of these AVC nozzles was also studied and we showed, with the use of a new four-square SPL-difference chart, how the noise benefits are inter-related to the installation effects. Thus, we verified, for example, that if the isolated noise benefit is higher than the installed noise benefit for a given modified nozzle, as is the case for the best nozzle, then its installation effect is worse than the baseline nozzle. The physical reasons for this effect through source diagnostics are taken up in Part 3.

It is due to the success of the quietest RT-nozzle with these model-scale T-fan chevrons, in both installed and isolated configurations, that we decided to verify its benefits, after appropriate aerodynamic performance tests, in a full-scale flight test, reported in Nesbitt et al[8] and Mengle et al[9].

Acknowledgments

References

[1] Janardan, B.A., Hoff, G.E., Barter, J.W., Martens, S., Gliebe, P.R., Mengle, V. and Dalton, W.N., "AST Critical Propulsion and Noise Reduction Technologies for Future Commercial Subsonic Engines – Separate-Flow Exhaust System Noise Reduction Concept Evaluation," NASA/CR-2000-210039, Dec. 2000.

[2] Mengle, V.G., "Jet Noise Characteristics of Chevrons in Internally Mixed Nozzles," AIAA Paper 2005-2934.

[3] Mengle, V.G., Elkoby, R., Brusniak, L. and Thomas, R., "Reducing Propulsion Airframe Aeroacoustic Interactions with Uniquely Tailored Chevrons. 1. Isolated Nozzles," AIAA Paper No. 2006-2467.

[4] Mengle, V.G., Elkoby, R., Brusniak, L. and Thomas, R., "Reducing Propulsion Airframe Aeroacoustic Interactions with Uniquely Tailored Chevrons. 3. Jet-Flap Interaction," AIAA Paper No. 2006-2935.

[5] Herkes, W.H., Olsen, R. and Uellenberg, S, "The Quiet Technology Demonstrator Program: Flight Validation of Airplane Noise Reduction Concepts," AIAA Paper No. 2006-2720.

[6] Fink, M.R., "Propulsive Lift Noise," in *Aeroacoustics of Flight Vehicles: Theory and practice. Vol. 1: Noise Sources*, edited by Hubbard, NASA RP-1258, Vol. 1, 1991, Ch. 8, pp. 449-481.

[7] Elkoby, R., "Full-Scale Propulsion Airframe Aeroacoustics Investigation," AIAA Paper No. 2005-2807.

[8] Nesbitt, E., Mengle, V.G., Czech, M., Callendar, B., and Thomas, R., "Flight Test Results for Uniquely Tailored Propulsion-Airframe Aeroacoustic Chevrons: Community Noise," AIAA Paper No. 2006-2438.

[9] Mengle, V.G., Ganz, U., Nesbitt, E., Bultemeier, E.J. and Thomas, R., "Flight Test Results for Uniquely Tailored Propulsion-Airframe Aeroacoustic Chevrons: Shockcell Noise," AIAA Paper No. 2006-2439.